Received 1 January 2006
Accepted 9 July 2006

Computational investigation of turbulent jet impinging onto rotating disk

A.C. Benim, K. Ozkan and M. Cagan
Department of Mechanical and Process Engineering, Duesseldorf University of Applied Sciences, Duesseldorf, Germany, and
D. Gunes
Mechanical Engineering Faculty, Istanbul Technical University, Istanbul, Turkey

Abstract

Purpose – The main purpose of the paper is the validation of a broad range of RANS turbulence models, for the prediction of flow and heat transfer, for a broad range of boundary conditions and geometrical configurations, for this class of problems.

Design/methodology/approach – Two- and three-dimensional computations are performed using a general-purpose CFD code based on a finite volume method and a pressure-correction formulation. Special attention is paid to achieve a high numerical accuracy by applying second order discretization schemes and stringent convergence criteria, as well as performing sensitivity studies with respect to the grid resolution, computational domain size and boundary conditions. Results are assessed by comparing the predictions with the measurements available in the literature.

Findings – A rather unsatisfactory performance of the Reynolds stress model is observed, in general, although the contrary has been expected in this rotating flow, exhibiting a predominantly non-isotropic turbulence structure. The best overall agreement with the experiments is obtained by the k-ω model, where the SST model is also observed to provide a quite good performance, which is close to that of the k-ω model, for most of the investigated cases.

Originality/value – To date, computational investigation of turbulent jet impinging on to "rotating" disk has not received much attention. To the best of the authors' knowledge, a thorough numerical analysis of the generic problem comparable with present study has not yet been attempted.

Keywords Turbulence, Jets, Rotational motion, Modelling

Paper type Research paper

Nomenclature

C_f = skin friction coefficient ($C_f = 2\tau_w/\rho U^2$)
d = jet diameter (m)
e = distance between jet and disk axes (m)
h = distance between jet exit to disk (m)
k = turbulence kinetic energy (m^2/s^2)
Nu_d = Nusselt number based on jet diameter ($Nu_d = \alpha d/\lambda$)
Nu_R = Nusselt number based on disk radius ($Nu_R = \alpha R/\lambda$)
Q_J = time averaged jet flow rate (m^3/s)
r = radial coordinate (m)
R = disk radius (m)
Re_D = disk Reynolds number ($Re_D = \Omega R^2/\nu$)
R_e = rotational Reynolds number defined by impingement radius ($Re_e = \Omega e^2/\nu$)
Re_J = jet Reynolds number ($Re_J = Ud/\nu$)
u, v, w = axial radial and azimuthal velocities (m/s)
U = time averaged bulk jet velocity
y = wall distance (m)

International Journal of Numerical Methods for Heat & Fluid Flow
Vol. 17 No. 3, 2007
pp. 284-301

0961-5539
DOI 10.1108/09615530710730157

y^+ = non-dimensional wall distance ($y^+ = (y/\nu)\sqrt{\tau_w/\rho}$)
z = distance from disk surface (axial coordinate) (m)

Greek symbols
α = time averaged heat transfer coefficient (W/m^{2}K)
β = ratio of Re numbers ($\beta = Re_J/Re_D$)
ε = dissipation rate of k (m^2/s^3)
λ = thermal conductivity (W/mK)
ν = kinematic viscosity (m^2/s)
ρ = density (kg/m^3)
τ_w = time averaged wall shear stress (Pa)
ω = turbulence frequency (1/s)
Ω = disk rotational speed (rad/s)

Superscripts
$()'$ = instantaneous value
$\overline{()}$ = time-averaged value

Abbreviations
RANS = Reynolds averaged Navier-Stokes equations
RSM = Reynolds stress model
SST = shear stress transport
WF = wall functions

Introduction

The turbulent impinging jet is of great importance in many engineering problems, concerning processes such as cooling, heating and drying. We are particularly interested in gas turbine cooling, as discussed in Benim *et al.* (2004). During the manufacture of gas turbines, a detailed insight of the heat transfer mechanisms is very important especially in designing the highly thermally stressed components such as the turbine disk. There is a variety of schemes used for this purpose, an overview of which is provided in Owen and Rogers (1989). An efficient disk cooling arrangement consists of squirting a cooling jet at the rotating disk. In pre-swirl systems, a similar flow situation can occur for some designs and operation conditions (Benim *et al.*, 2004; Owen and Rogers, 1989). Thus, the present work focuses on the generic problem of turbulent jet impinging onto a rotating disk, for assessing the predictive capability of computational procedures in such applications.

Owing to vast applications, many experimental and computational studies have been reported on turbulent impinging jets. Most of them consider the problem of impinging jet onto a stationary surface with or without cross flow (Jambunathan *et al.*, 1992; Cooper *et al.*, 1993; Craft *et al.*, 1993; Behnia *et al.*, 1999).

However, the case of jet impingement onto a rotating surface exhibits different characteristics. The boundary layer established by disk rotation and pumping attaining its maximum velocity at the wall is skewed, and subject to a centrifugal force field.

A comparably smaller amount of experimental work has been published on the problem of turbulent jet impinging on a rotating surface. Earlier studies, such as those of Metzger and Grochowsky (1977), Popiel and Boguslawski (1986) and Metzger *et al.* (1989) were mainly concentrated on heat transfer measurements and some flow visualization. Rather recently, more detailed LDA measurements of the flow field, including turbulence statistics have been published in Brodersen *et al.* (1996) and Minagawa and Obi (2003).

Computational investigation of the phenomenon has received an even smaller attention. To the best of the authors' knowledge, a thorough numerical analysis of the generic problem has not yet been attempted. Thus, the purpose of the present study is the computational investigation of the generic problem of turbulent jet impinging onto

a rotating disk, and a validation of the computational procedures by comparisons with the available experiments.

An overview of the applied mathematical and numerical modeling

For numerical investigations, the general-purpose CFD code Fluent (2004) has been used as basis, which utilizes a finite volume method to discretize the governing equations, and a pressure-correction formulation to handle the velocity-pressure coupling. The Reynolds (*Re*) averaged continuity, Navier-Stokes and convective-diffusive energy transport (modeled according to *Re*'s analogy) equations (Durbin and Reif, 2003) have been solved for the incompressible, *quasi-steady*, turbulent flow, together with the additional transport equations for the turbulence quantities. For the material properties, constant values have been used, which correspond to a mean temperature of the considered problem.

Within the framework of a RANS formulation, a broad range of two-equation turbulence models, namely, the standard (Launder and Spalding, 1974), the RNG (Yakhot and Orszag, 1986) and realizable (Shih *et al.*, 1995) k-ε models, as well as the k-ω model (Wilcox, 1993), and the SST model (Menter, 1994) have been used. Additionally, the *Re* Stress Model (RSM), using a quadratic modeling of the pressure-strain term (Speziale *et al.*, 1991), has been investigated. Mainly, the low *Re* number (low-*Re*) versions (Shima and Launder, 1989) of the models have been applied, adopting amendments such as the two-layer-zonal approach (Wolfstein, 1969), which are able to resolve the near-wall region. For comparison, high-*Re* number (high-*Re*) versions (Launder and Spalding, 1974) of some models have also been applied adopting a wall-function approach (WF) for the near-wall flow. For this purpose, the non-equilibrium wall functions (Kim and Choudhury, 1995) have been employed, which are principally superior to the standard ones (Launder and Spalding, 1974). For all applications, always the original sets of model constants have been used. In generating the computational grids, special care has been taken for a convenient near-wall resolution, resulting in adequate near-wall y^+ values, which are compatible with the assumptions of the respective turbulence model (Benim and Arnal, 1994).

A second order upwind scheme (Barth and Jespersen, 1989) has been used for the discretization of the convective terms of the governing equations of all convective diffusively transported variables, for attaining a high numerical accuracy (for *Re* stress components, a first-order scheme has been used for some cases).

Test cases

The investigated test cases have been based on the experiments of Minagawa and Obi (2003) (MO), Popiel and Boguslawski (1986) (PB) Metzger *et al.* (1989) (MBB) and Metzger and Grochowsky (1977) (MG). The generic configuration of the disk and jet arrangements for the test cases with the indication of boundary types conditions are shown in Figure 1.

Table I summarizes the geometric parameters and operation conditions for the investigated test cases. Please note that the cases MG-1 and MG-2, each, represent 5-6 cases with varying jet *Re* number for a given disk *Re* number.

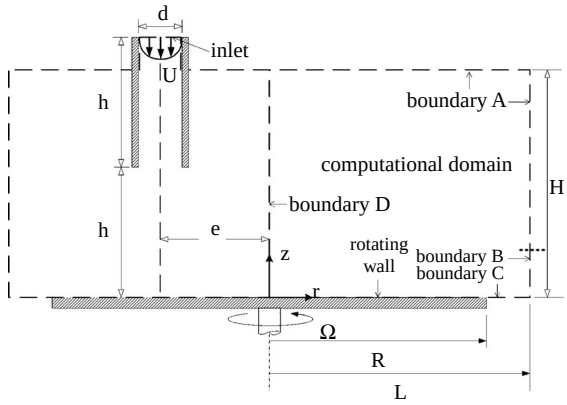

Figure 1.
Geometry, solution domain, boundaries

Boundary conditions

The applied boundary types are shown in Figure 1 and Table I. At the inlet of the jet flow (Figure 1), all variables (velocity components, turbulence quantities, temperature) are prescribed. In all experiments, quite long lances were used, so that practically fully developed conditions towards the end of the pipe should be expected. Thus, the prescription of an empirical turbulent fully developed pipe flow velocity profile (e.g. 1/7 law) at the domain inlet (Figure 1) could be thought to provide sufficient accuracy. Nevertheless, instead of this approach, the boundary conditions at the domain inlet (Figure 1) have been obtained by preliminary computations of the developing pipe flow problem, separately for each case, and for each turbulence model used, aiming at an even higher accuracy of the inlet boundary conditions, especially for the various turbulence quantities required by different turbulence models. In these preliminary computations of the developing pipe flow, uniform distributions have been applied at the inlet of the pipe, using the experimentally known velocities and temperatures, and assuming a turbulence intensity of 4 percent and a mixing length of 30 percent pipe diameter. An inspection of Table I shows that the jet *Re* number indicates a laminar flow within the pipe, for a few cases of MG-1 and MG-2 (where, but, the flow becomes turbulent in the outer region, near the rotating disk). In computing those cases, using low-*Re* turbulence models, a very low turbulence intensity has been prescribed at the pipe inlet (0.1 percent) in order to cope with this situation. For better accounting for a possible interaction of the jet flow with the flow in the outer domain, in the vicinity of the jet exit, the inlet boundary of the solution domain has not been placed exactly at the jet outlet, but at a certain distance upstream. The latter has normally been taken to be equal to the jet-to-disk-distance h (Figure 1), which was taking values about 2-5d (Table I).

At the disk wall, the rotational velocity and the wall temperature have been prescribed, as these values were provided by the experiments. The jet-disk arrangements were placed in quite large plenums for most of the experiments, namely for those of Minagawa and Obi (2003), Popiel and Boguslawski (1986) and Metzer and Grochowsky (1977) (characteristic dimension of the confining box much larger than the disk diameter (ten times, or more)). Thus, for these cases, the effect of the confinement can be neglected and the configuration can be assumed to be free in space.

Case	h/d	R/d	e/R	Modeling	h/H	R/L	bd.A	bd.B	bd.C	bd.D	Re_J	Re_D
MO-1	5	6	0	2D	0.5	<1	p	p	s	s	14,500	235,650
MO-2	5	6	0	2D	0.5	<1	p	p	s	s	14,500	251,400
PB-1	5	7.56	0	2D	0.5	<1	p	p	s	s	178,000	1,209,600
PB-2	5	7.56	0	2D	0.5	<1	p	p	s	s	46,000	1,209,600
MBB-1	2.13	21.3	0	2D	1	1	w	o	w	s	23,170	271,000
MBB-2	2.13	21.3	0	2D	1	1	w	o	w	s	23,170	464,000
MG-1	2	10	0.8	3D	0.5	<1	p	p	s	i	200-20,000	40,000
MG-2	2	10	0.8	3D	0.5	<1	p	p	s	i	200-20,000	120,000

Table I.
Definitions of the investigated cases

Notes: Abbreviations: MO, Minagawa and Obi (2003); PB, Popiel and Boguslawski (1986); MBB, Metzger *et al.* (1989); MG, Metzger and Grochowsky (1977); o, outlet boundary; p, pressure boundary; s, symmetry axis or plane; w, solid wall; i, domain interior

Consequently, in computations based on these experiments, instead of modeling the whole plenum geometry, which would require an unnecessarily too large grid, a cylindrical section (radius $= L$, height $= H$, Figure 1) around the apparatus has been defined as the solution domain. The enclosure of this domain is, then, has been declared to be pressure boundaries (Table I), with a prescribed constant ambient pressure. This is expected to be an accurate enough formulation, provided that the pressure boundaries are placed sufficiently far away from the impingement region. The latter has been ensured by preliminary computations.

At the pressure boundaries, the ambient values of the temperature and turbulence quantities need additionally to be prescribed, since, there, an entrainment of the ambient fluid across these boundaries is expected. As the temperature is given by the experiments, uncertainties exist for the turbulence quantities. For the latter, a turbulence intensity of 1 percent and a viscosity ratio (turbulent viscosity divided by laminar viscosity) of 1 have been assumed. Additional computations have been performed by reducing and increasing these values within reasonable ranges, where no remarkable changes of the results have been observed. This confirms the relative insensitivity of the results on these quantities around the prescribed values, and, thus, the convenience of the prescribed values.

In the experiments of Metzger *et al.* (1989), the jet-disk arrangement was placed in a rather small confinement, where the walls of the confining box was aligned with the disk edge and the jet outlet. For this case, the boundaries of the enclosure (Figure 1) have been defined to be solid walls (Table I), of course, where an outlet boundary has also been modeled as a part of the boundary (Figure 1) aligning with the disk edge, according to the geometry given in Metzger *et al.* (1989).

In all considered test cases, except those based on the experiments of Metzger and Grochowsky (1977), co-axial jet and disk arrangements have been considered. These test cases give rise to a 2D-axisymmetric problem formulation, which has been utilized in the computations, of course (Figure 1, Table I). In the test cases based on the experiments of Metzger and Grochowsky (1977), the jet and the disk have not been co-axial, but eccentric. Thus, for these test cases, a 3D analysis have been applied (Figure 1, Table I).

Grid generation

Structured grids have been employed. Special care has been taken for obtaining adequate y^+ values for near-wall cells. For low-*Re* turbulence model applications, grids in near-wall regions have been constructed so fine that sufficiently small local y^+ values have been obtained. For all such applications, the local y^+ values have been varying between the minimum of ~ 0.1 and maximum of ~ 0.5, having the value of ~ 0.3 in the mean. In addition, a rather mild grid expansion has been applied, which resulted in a quite fine resolution of the near-wall layer (about ten cells in the region $0 < y^+ < 5$). For high-*Re* turbulence model applications with WF, the near-wall grid has been made coarse enough to obtain sufficiently large y^+ values. For these applications, the local y^+ values have been varying between the minimum of ~ 20 (rather small regions) and a maximum of ~ 100, exhibiting a mean value of ~ 70.

A grid independency study has been performed for the 2D-axissymmetric case of MO-1 (Table I), using 100×100, 200×200, 300×300 and 400×400 grid resolutions (using the SST model). It has been observed that even 100×100 grid provides a sufficient grid independency, provided that the wall layers are resolved adequately and a second order discretization scheme is used. However, for excluding any uncertainty, computations have been performed using the finer, 300×300 grid for the 2D cases, where the total number of grid points were not that critical with respect to the computational overhead. Here, the grid lines have been concentrated in the impingement area, with a mild expansion ratio in the radial direction beyond this region. In the axial direction, 200 cells have been used for the region between the jet exit position and the disk and 100 cells for the region between the pressure boundary and the jet exit location. A formal grid independency study has not been performed for the remaining cases, where the construction of the grids have been led by the experience gained for the first case and the by the requirements of obtaining an adequate near-wall resolution. For the 2D cases (MG.1, MG-2, Table I) a grid consisting about 800,000 cells has been used, some views of which are shown in Figure 2.

Convergence criteria

Special attention has been paid to obtain results with a high convergence level. The default convergence criterion of fluent is that scaled residuals of all equations fall below 10^{-3}, whereas a tolerance of 10^{-6} is required for the energy equation. In the present computations 100 times smaller tolerances have been required. For some RSM computations, it was not possible to obtain that low residual values, although a reasonable convergence, well below the default tolerances, was, in any case, obtained. For such cases, additional transient runs were performed to ensure this behavior were not due to an eventual suppression of any important transient phenomena. In any case, upon the fulfillment of the respective convergence criteria, before judging for the convergence, several hundreds of additional iterations have been performed for ensuring that all important variables do not show any significant changes more. The final results have been obtained using rather high under-relaxation factors (velocities: 0.7, k, ε, ω: 0.8, *Re* stresses: 0.5, other variables: 1.0).

Results

Applying the above-mentioned turbulence models to the test cases summarized in Table I, a rather huge amount of data has been produced. A limited selection will be

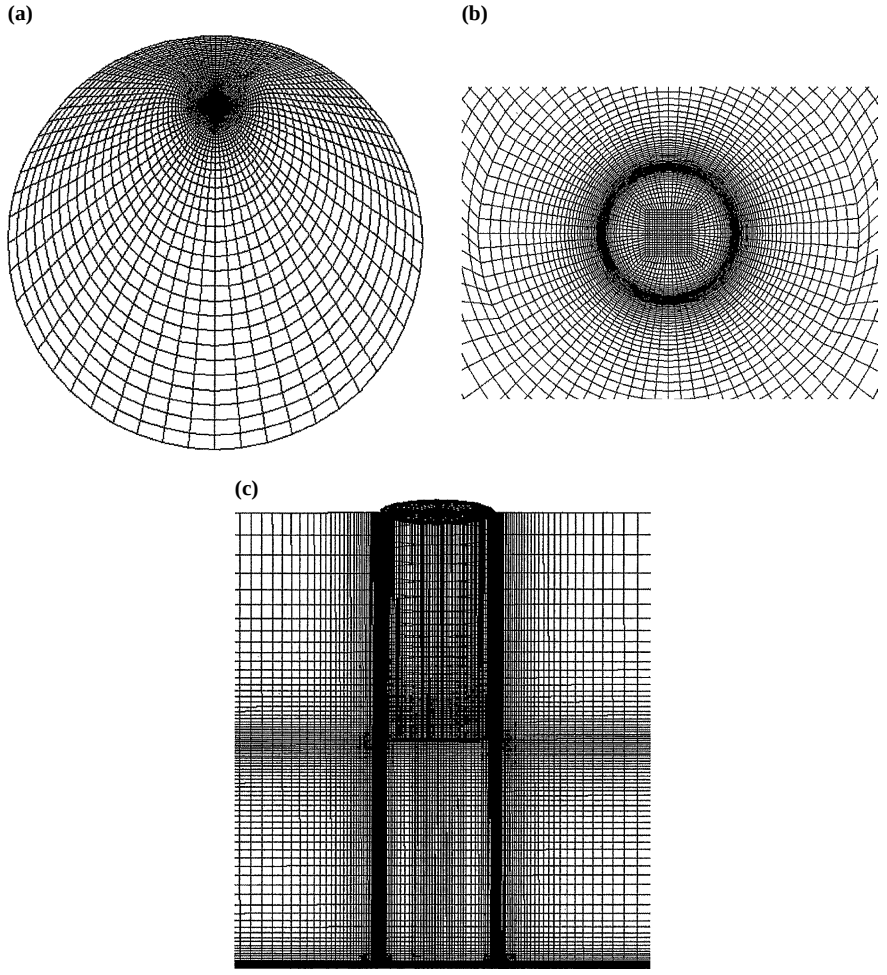

Figure 2.
The 3D grid (a) disk surface grid; (b) detail of impingement region; (c) grid distribution in axial direction

presented here. The results of the standard, realizable and the RNG versions of the k-ε model were mostly quite similar, whereas the RNG version has been observed to provide slightly better results for some cases. Thus, here, only the RNG version results are presented for the k-ε model, which are designated as "k-ε" in figure legends. For all models, the presented results are the ones, obtained using the low-Re versions of the models, resolving the near-wall regions, with one exception: results using the wall-functions are additionally presented only for the high-Re, k-ε model, for comparison, which are designated as "k-ε-WF" in figure legends.

Cases MO-1, MO-2

For the test cases MO-1 and MO-2 (Table I) based on the measurements of Minagawa and Obi (2003), experimental data were available for velocities and turbulence

quantities. Heat transfer measurements were not performed. Radial profiles of the radial velocity along an axial section at $z/d = 0.032$ are shown in Figure 3, for the case MO-1.

All models underestimate the peak velocity around $r/d = 1$, where the k-ω model shows the best agreement with the experiments. The largest discrepancy for the peak velocity is observed for the k-ε model, which predicts a rather flat variation throughout. The k-ε -WF (high-*Re*) results are poorer compared to the k-ε (low-*Re*) ones. In this comparison (k-ε vs k-ε-WF) the discrepancy is rather small. But, please note that the displayed results for k-ε-WF are the cell-center values of near-wall cells, but not their (linear) interpolation to the wall (this is thought to be rather in the sense of the wall-functions philosophy, which, strictly speaking, would require a logarithmic interpolation). The SST model shows the second best agreement with the experiments, exhibiting a performance between k-ε and k-ω models, as one would expect. The peak velocity captured by RSM is similar to that of the SST model, and, thus, shows a better agreement with experiments than the k-ε model. However, at larger radii, RSM shows a poorer agreement with experiments (Figure 3).

Variations of radial velocity with z/d, at the radial position $r/d = 5.8$, for a slightly increased disk speed (MO-2, Table I) are shown in Figure 4.

An inferior agreement with the experiments is shown by k-ε-WF (the curve is drawn up to the center of the near-wall cell, but not between the cell-center and the wall). Among the low-*Re* models, the k-ε model performs inferiorly compared to the others. In predicting the near-wall peak value, the k-ω model shows the best performance, which, however, exhibits a deviation from the measured values for larger z/d. The SST model under-predicts the near-wall peak value compared to the k-ω model, but shows a better performance at higher z/d. The near-wall peak value is well predicted by RSM, which, however, over-predicts the measurements away from the wall (Figure 4).

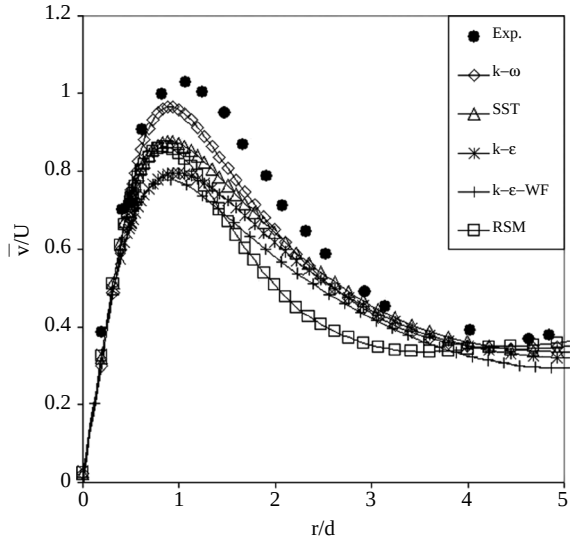

Figure 3.
Radial variation of near-wall radial velocity at $z/d = 0.032$ (MO-1)

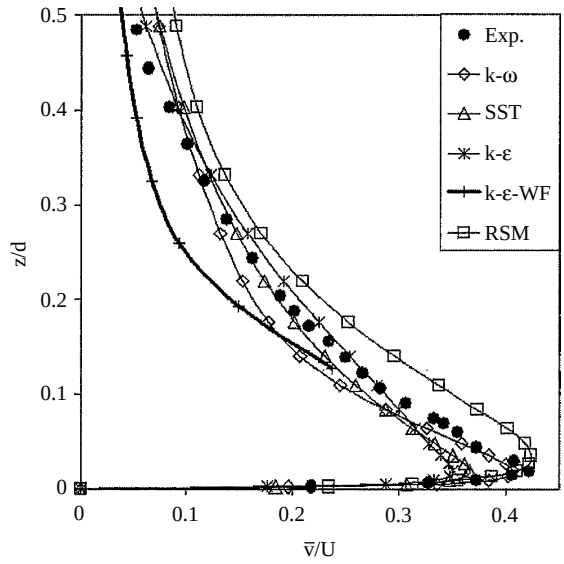

Figure 4.
Radial velocity as function of z/d at $r/d = 5.8$ (MO-2)

Axial profiles of the normal components of the *Re* stresses, as predicted by RSM, at the radial position $r/d = 5.8$, for the case MO-2 are shown in Figure 5.

Although a qualitative agreement of the predicted *Re* stresses with the measurements can still be claimed in so far that the tangential component is predicted to be larger than the other components, which is qualitatively in agreement with the measured vales, it is obvious that the measured strong anisotropy of the *Re* stresses is strongly underpredicted by RSM, quantitatively (Figure 5).

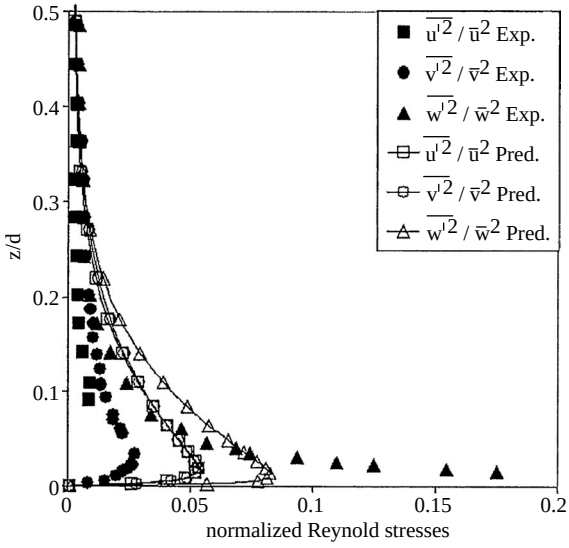

Figure 5.
Reynolds stresses as function of z/d at $r/d = 5.8$ (MO-2)

Cases PO-1, PO-2

For the test cases PB-1 and PB-2 (Table I) based on the experiments of Popiel and Boguslawski (1986), heat transfer measurements were available, whereas velocity field measurements were not presented. Radial variations of the *Nu* number along the disk surface are shown in Figure 6, for the case PB-1.

The k-ω and SST models show the best overall agreement with the experiments. The SST model performs better in predicting the peak values in the impingement region, whereas the k-ω model show a better agreement with the measurements for larger radii. Greater discrepancies between the models are observed rather in the central, i.e. in the core of the impingement region. For higher values of r/d, all models predict rather quite close values and slightly overpredict the experiments, except the k-ω model, which shows a better performance (Figure 6) throughout.

Figure 7 shows the radial variation of the *Nu* number along disk surface for the case PB-2.

Also for this case, the predictions obtained by different models show the largest discrepancies between each other in the central, stagnation region, in the vicinity of $r/d = 0$. For all values of r/d, the SST model shows the best agreement with the experiments. The k-ω model delivers quite close results to the SST ones, and shows, quite closely, the second best agreement. For intermediate values of the radius, i.e. for approx. $1.5 < r/d < 4.5$, the experiments show a local minimum, where the *Nu* number first decreases up to $r/d \approx 3$, and then increases again, quite abruptly. None of the models could sufficiently predict this behavior. RSM may be considered to show a weak qualitative similarity to this variation, which, however, shows a strong underprediction at low radii, and an overprediction at large radii, quantitatively (Figure 7). A much better performance of the RSM was expected at the beginning of the present study, since it can cope much better with the predominantly non-isotropic turbulence structure of swirling flows compared to the turbulence viscosity-based models.

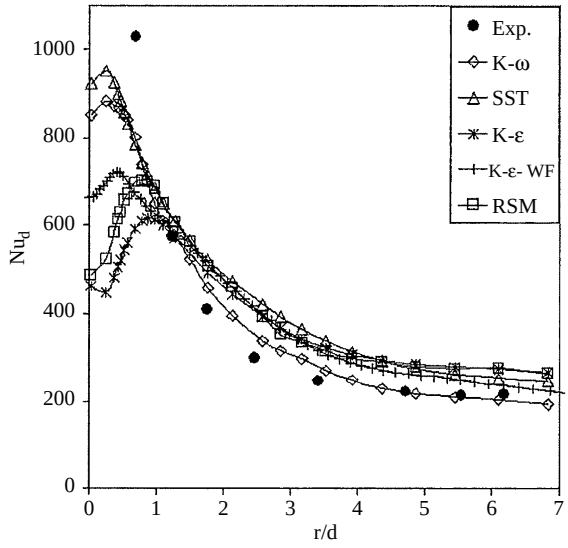

Figure 6.
Radial variation of *Nu* number along disk surface (PB-1)

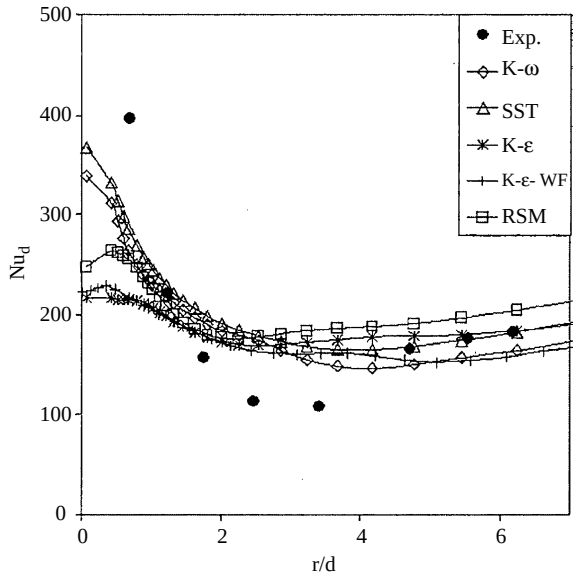

Figure 7.
Radial variation of *Nu* number along disk surface (PB-2)

Thus, the present comparably rather poor performance of RSM (Figures 3-7) is an unexpected behavior, an explanation of which would require further analysis and more detailed comparisons with turbulence data. Within the present study, additional RSM computations have been performed using the linear (Launder *et al.*, 1975) modeling of the pressure-strain term, with and without considering the so-called wall reflection terms, which have led to no improvement of the RSM performance.

A inspection of the boundary conditions of the cases PB-1 and PB-2 (Table I) implies that rotational effects in comparison to impingement effects should be greater for the case PB-2 compared to the case PB-1, as the jet *Re* number of the latter is smaller than that of the former for the same disk *Re* number. The discrepancies in the central stagnation region put aside, the discrepancies between the measurements and the predictions for larger radii, which are observed to be larger for PB-2, may be attributed to the stronger rotational effects for this case.

For this co-axial arrangement, it is obvious that the effects of rotation start to dominate at a certain distance away from the axis, whereas the near-field of the jet impingement region is expected to be impingement dominated. In Popiel and Boguslawski (1986), the following empirically-based expression:

$$\frac{r}{d} = \frac{Re_J}{Re_D}\left(\frac{R}{d}\right)^2\left[1 - 2\times 10^{-4}\left(Re_J\right)^{2/3}\right] \tag{1}$$

was suggested for defining the transition point between the impingement and rotation dominated regions, depending in the *Re* numbers and the geometries of the jet and the disk. According to this criterion, the transition form the impingement dominated region to the rotation dominated region occurs at $r/d \approx 3.1$, for the case PB-1 and at $r/d \approx 1.6$, for PB-2. These numbers may be considered to show some correspondence to the regions where rather larger discrepancies between the predictions and

measurements occur or start to occur are observed at larger radii, which is especially apparent for the more strongly rotation dominated case PB-2 (Figure 7).

The radial distribution of the predicted skin friction coefficient for the case PB-2 is shown in Figure 8.

One can observe that the skin friction curve shows a local minimum at $r/d \approx 1.6$, which corresponds quite well with the criteria given by equation (2) for the transition position from the impingement dominated regime into the rotation dominated one. This finding may be seen to imply that the transition location between the impingement and rotation dominated regimes is indicated by the local minimum of the wall shear stress. In Figure 8, the results for the impinging jet with a stationary disk (A) and the rotating disk without a jet (B), as well as the superposition of A and B are also plotted, for comparison. It is interesting to note that the superposition of the cases A (jet with stationary disk) and B (rotating disk without jet) produces a curve very close to the curve obtained for the "combined" problem of impinging jet onto the rotating disk, i.e. for the case PB-2 (Figure 8).

Cases MBB-1, MBB-2

For the test cases MBB-1 and MBB-2 based on the experiments of Metzger *et al.* (1989), the jet-disk arrangement was placed in a low confinement (Table I), resulting in a different flow situation (Table I) than that of a free-disk arrangement of all other test cases. Predicted and measured radial variations of the *Nu* number along disk surface are shown in Figures 9 and 10.

For the case MBB-1 (Figure 9), with comparably lower disk *Re* number (lower rotational effects), the predictions obtained by all turbulent viscosity-based models lie quite close to each other, which show a rather good agreement with the measurements.

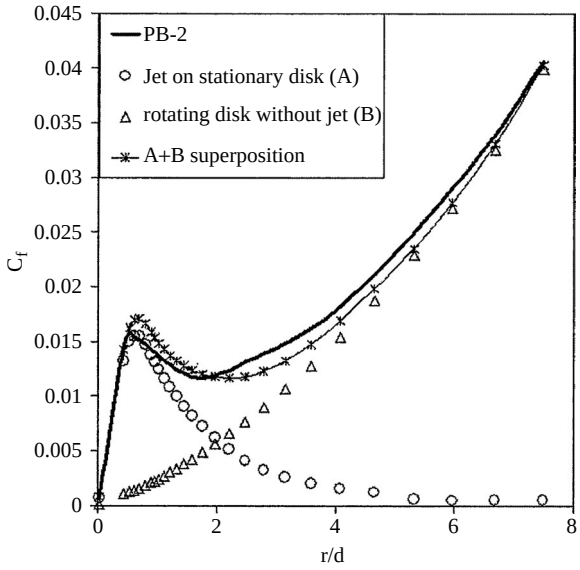

Figure 8.
Radial variation of skin friction coefficient along disk surface (PB-2)

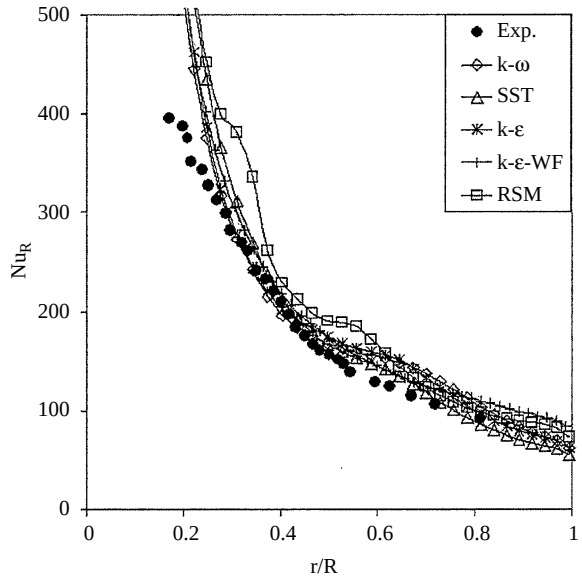

Figure 9.
Radial variation of *Nu* number along disk surface (MBB-1)

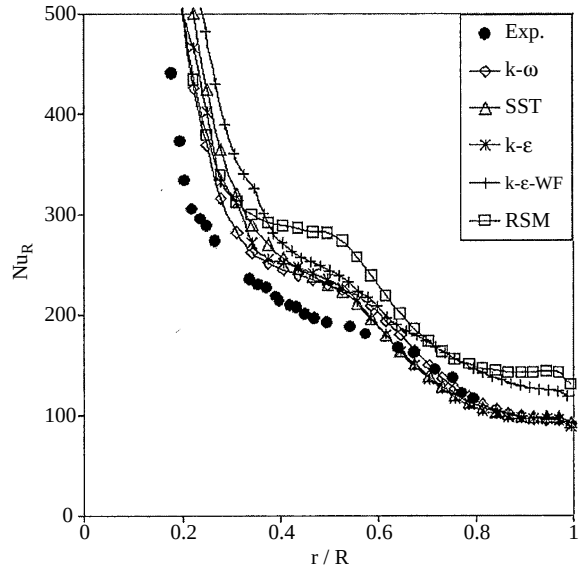

Figure 10.
Radial variation of *Nu* number along disk surface (MBB-2)

The results of the RSM show deviations from the experiments and the rest of the predictions, qualitatively and quantitatively (Figure 9).

For the case MBB-2 (Figure 10), with higher disk *Re* number (higher rotational effects), all low-*Re* turbulence viscosity-based models show a similar agreement to each other, which, however, show a greater discrepancy from the measurements compared

to the previous case (MBB-1, Figure 9). The high-*Re*, *k*-ε model with wall functions show a deviation form the results of the low-*Re* models and a greater discrepancy to the experiments. The discrepancy to the experimental results become even larger using the RSM (Figure 10).

Cases MG-1, MG-2

The test cases MG-1 and MG-2, which are based on the experiments of Metzger and Grochowsky (1977) majorly differ from the previous ones through the fact that the jet and disk are arranged eccentrically (Figure 1, Table I). Thus, a 3D problem arises. The modes of interaction between the jet and the disk become also different, where the rotational effects may be dominating even at the impingement position, depending on the *Re* number ratio. For the present test cases, only the models have been applied, which consistently have shown the best overall agreement with the predictions so far, namely the *k*-ω and SST models. Metzger and Grochowsky (1977) did not provide measurements of the velocity field. However, some velocity field data on a different, but quite similar test rig was provided by Brodersen *et al.* (1996), which are used, here, for a qualitative comparison. Figure 11 shows the measured (Brodersen *et al.*, 1996) and predicted velocity vector fields in a plane close to disk surface ($z/d = 0.03$) for different values of the *Re* number ratio β.

Although the experimental and computational *Re* number ratios are not identical, similar qualitative trends are indicated by the predictions and the experiments. For small values of β the jet does not seem to fully penetrate into the wall boundary layer. With increasing β the jet becomes more capable of disturbing the wall flow and is able to expand even in against the direction of disk rotation. Metzger and Grochowsky (1977) had also performed flow visualization experiments (which, however, were not

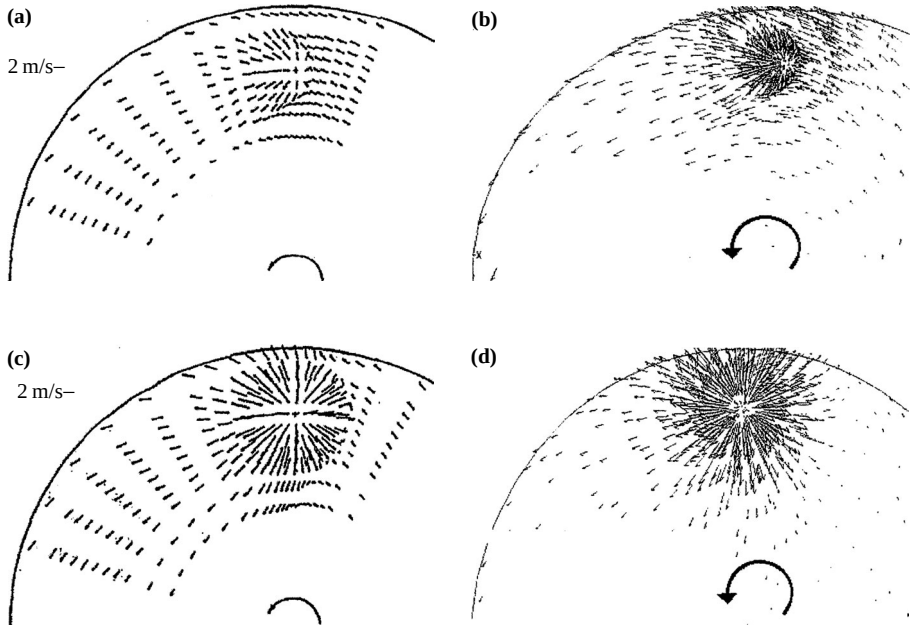

Figure 11.
Velocity vector fields at $z/d = 0.03$: (a) experiments (Brodersen *et al.*, 1976), $\beta = 0.0724$; (b) present prediction, $\beta = 0.056$; (c) experiments (Brodersen *et al.*, 1976), $\beta = 0.1306$; (d) present prediction, $\beta = 0.128$

documented in their paper) and defined "impingement dominated" and "rotation dominated" regimes, depending on the resulting velocity patterns, where a strong jet penetration (similar to Figure 11(c) and (d)) is used to define the "impingement dominated" regime, whereas a weak penetration and a strong deflection of the jet (similar to Figure 11(a) and (b)) is used to mark the "rotation dominated" regime. They have found that the transition between the two regimes correlates to the flow rate ratio Q_J/Q_P, where Q_P is defined to be the empirical "pumping flow rate" at the impingement radius for a free rotating disk, which is given by Schlichting (1968) as:

$$Q_P = 0.886\pi\nu e Re_e^{0.5} \tag{2}$$

The transitional values of Q_J/Q_P were found to additionally depend on the rotational *Re* number (Metzger and Grochovsky, 1977).

For the present test cases, the experimental *Nu* numbers (Metzger and Grochowsky, 1977) were provided as average values for the whole disk surface. Figures 12 and 13 display the predicted and measured *Nu* numbers (average values for the whole disk surface) as a function of the flow rate ratio Q_J/Q_P, for the cases MG-1 and MG-2, respectively. In the figures, the impingement and rotation dominated regimes after Metzger and Grochowsky (1977) are also indicated.

For the case MG-1, with lower disk *Re* number one can observe (Figure 12) that the *k-ω* and SST model predictions are quite close to each other and show a similar agreement with the experiments. For the case MG-2, with higher disk *Re* number, the *k-ω* model show throughout a much better agreement with the experimental values than the SST model. In both cases, the predictions agree better with the experiments in the impingement dominated regime, compared to the rotation dominated regime and the transition zone.

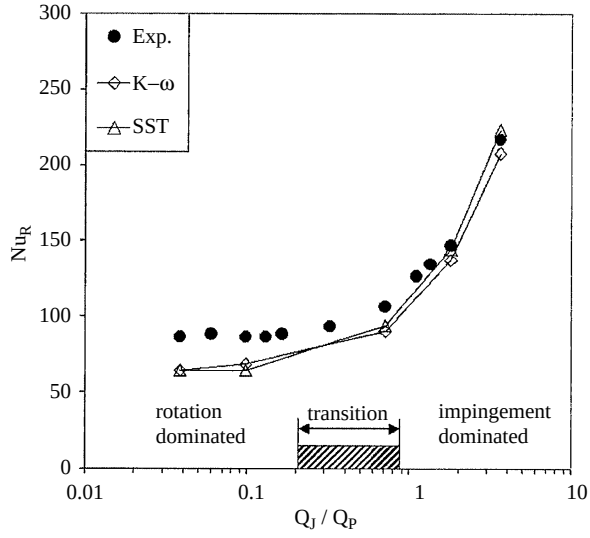

Figure 12.
Variation of average disk *Nu* number with Q_J/Q_P (MG-1)

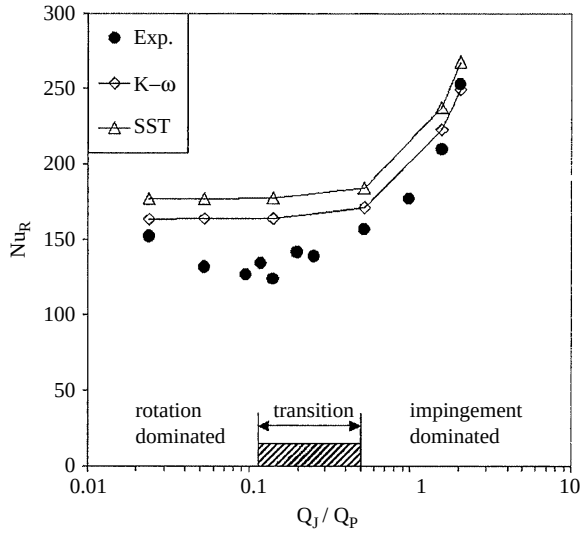

Figure 13.
Variation of average disk *Nu* number with Q_J/Q_P (MG-2)

Conclusions

Flow and heat transfer for turbulent jet impinging onto rotating disk have computationally been investigated, using different turbulence models. Co-axial and eccentric arrangements of the jet and the disk have been analyzed, which resulted in 2D axisymmetric and 3D formulations. Results have been compared with the experiments. It has also been demonstrated/confirmed that the low-*Re* turbulence models resolving the wall-layer are potentially superior to the high-*Re* models based on wall functions, as this discrepancy has been quantified within the framework of the test cases. The best overall agreement with the experiments has been observed to be provided by the *k-ω* model, where the SST model has been observed to show a similar overall performance for most of the cases. It has been observed that the agreement between the predictions and measurements generally deteriorates for increasing rotational effects, i.e. in rotation dominated regimes and cases, as well as in transitional regimes between impingement and rotation dominated zones. It was initially expected that the RSM would provide a superior performance especially for these cases, since it can much better accommodate for the non-isotropic turbulence structure dominating the rotational flows. The presents results have shown, however, that RSM performed, on the contrary, generally poorer compared to the turbulence viscosity-based models. The investigation of the reasons for this unexpected behavior, which would require a more detailed comparisons with turbulence data, is intended to be performed as part of the future work.

References

Barth, T.J. and Jespersen, D. (1989), "The design and application of upwind schemes on unstructured meshes", AIAA Paper: AIAA-89-0366.

Behnia, M., Parneix, S., Shabany, Y. and Durbin, P.A. (1999), "Numerical study of turbulent heat transfer in confined and unconfined impinging jets", *International Journal of Heat and Fluid Flow*, Vol. 20, pp. 1-9.

Benim, A.C. and Arnal, M. (1994), "A numerical analysis of the labyrinth seal flow", in Wagner, S., Hirschel, E.H., Périaux, J. and Piva, R. (Eds), *Computational Fluid Dynamics'94*, Wiley, New York, NY, pp. 839-46.

Benim, A.C., Brillert, D. and Cagan, M. (2004), "Investigation into the computational analysis of direct-transfer pre-swirl systems for gas turbine cooling", ASME Paper: ASME-GT2004-54151.

Brodersen, S., Metzger, D.E. and Fernando, H.J.S. (1996), "Flows generated by the impingement of a jet on a rotating surface: Part I – basic flow patterns", *ASME Journal of Fluids Engineering*, Vol. 118, pp. 61-7.

Cooper, D., Jackson, D.C., Launder, B.E. and Liao, G.X. (1993), "Impinging jet studies for turbulence model assessment – I. Flow-field experiments", *International Journal of Heat and Mass Transfer*, Vol. 36, pp. 2675-84.

Craft, T.J., Graham, R.H. and Launder, B.E. (1993), "Impinging jet studies for turbulence model assessment – II. An examination of the performance of four turbulence models", *International Journal of Heat and Mass Transfer*, Vol. 36, pp. 2685-97.

Durbin, P.A. and Reif, B.A.P. (2003), *Statistical Theory and Modelling for Turbulent Flows*, Wiley, New York, NY.

Fluent (2004), "Fluent 6.1", *User Manual*, Fluent Inc., Lebanon, NH.

Jambunathan, K., Lai, E., Moss, M.A. and Button, B.L. (1992), "A review of heat transfer data for single circular jet impingement", *International Journal of Heat Fluid Flow*, Vol. 13, pp. 106-15.

Kim, S.E. and Choudhury, D. (1995), "A near wall treatment using wall functions sensitised to pressure gradient", *Separated and Complex Flows ASME FED*, Vol. 217.

Launder, B.E. and Spalding, D.B. (1974), "The numerical computation of turbulent flows", *Computer Methods in Applied Mechanics and Engineering*, Vol. 3, pp. 269-89.

Launder, B.E., Reece, G.J. and Rodi, W. (1975), "Progress in the development of a Reynolds-stress turbulence closure", *Journal of Fluid Mechanics*, Vol. 68, pp. 537-66.

Menter, F.R. (1994), "Two equation eddy-viscosity turbulence models for engineering applications", *AIAA Journal*, Vol. 32, pp. 1598-695.

Metzger, D.E. and Grochowsky, L.D. (1977), "Heat transfer between an impinging jet and a rotating disk", *ASME Journal of Heat Transfer*, Vol. 99, pp. 663-7.

Metzger, D.E., Bunker, R.S. and Bosch, G. (1989), "Transient liquid crystal measurement of local heat transfer on a rotating disk with jet impingement", ASME Paper: ASME-89-GT-287.

Minagawa, Y. and Obi, S. (2003), "Turbulence impinging jet onto a co-axial rotating disk", in Hanjalic, K., Nagano, Y. and Tummers, M.J. (Eds), *Turbulence, Heat and Mass Transfer 4*, Begell House, New York, NY, pp. 747-54.

Owen, J.M. and Rogers, R.H. (1989), *Flow and Heat Transfer in Rotating Disk Systems, Vol. I: Rotor-Stator Systems*, Wiley, New York, NY.

Popiel, C.O. and Boguslawski, L. (1986), "Local heat transfer from a rotating disk in an impinging round jet", *ASME Journal of Heat Transfer*, Vol. 108, pp. 357-64.

Schlichting, H. (1968), *Boundary Layer Theory*, 6th ed., McGraw-Hill, New York, NY.

Shih, T.H., Liou, W.W., Shabbir, A., Yang, Z. and Zhu, J. (1995), "A new k-ε eddy-viscosity model for high Reynolds number turbulent flows – model development and validation", *Computers & Fluids*, Vol. 24, pp. 227-38.

Shima, N. and Launder, B.E. (1989), "Second moment closure for the near-wall sublayer: development and application", *AIAA Journal*, Vol. 27, pp. 1319-25.

Speziale, C.G., Sarkar, S. and Gatski, T.B. (1991), "Modelling the pressure-strain correlation of turbulence: an invariant dynamical systems approach", *Journal of Fluid Mechanics*, Vol. 227, pp. 245-72.

Wilcox, D.C. (1993), *Turbulence Modeling for CFD, Technical Report*, DCW Industries Inc., La Canada, CA.

Wolfstein, M. (1969), "The velocity and temperature distribution of one-dimensional flow with turbulence augmentation and pressure gradient", *International Journal of Heat and Mass Transfer*, Vol. 12, pp. 301-18.

Yakhot, V. and Orszag, S.A. (1986), "Renormalization group analysis of turbulence: I. Basic theory", *Journal of Scientific Computing*, Vol. 1, pp. 1-51.

Corresponding author
A.C. Benim can be contacted at: alicemal.benim@fh-duesseldorf.de